energies

MDPI

Article

Day-Ahead Operation Optimization of a Microgrid with a Micro Gas Turbine, Ground-Source Heat Pump and Photovoltaics for Office Buildings

Qian Zhang *, Reyhaneh Banihabib and Mohsen Assadi *

Department of Energy and Petroleum Engineering, University of Stavanger, 4036 Stavanger, Norway
* Correspondence: zq222788@hotmail.com (Q.Z.); mohsen.assadi@uis.no (M.A.)

Abstract

Day-ahead scheduling allows a microgrid to lower its operating cost by shifting between on-site generation and grid import according to hourly electricity prices. The benefit of such scheduling also depends on how the dispatchable units are represented, including their part-load behavior. This paper presents a day-ahead operation optimization of a grid-connected microgrid with a micro gas turbine (MGT), a ground-source heat pump (GSHP) and photovoltaics (PV) supplying the electricity and heating demand of an office building in Stavanger, Norway. A data-driven MGT model, trained on measured Ansaldo Energia T100 data, is coupled with validated Modelica models of the borehole heat exchanger, the heat pump and the PV array, so that the off-design performance of the turbine is retained in the scheduling problem. A genetic algorithm determines the hourly set-point and on-off status of the MGT over 24 h, using day-ahead electricity prices. The optimized schedule is compared with rule-based control for two representative days with high and low heating demand. Day-ahead optimization reduces the daily operating cost by 13% and 33.8%, respectively, by concentrating turbine operation in high-price hours. The share of recoverable waste heat that is usefully employed rises from 53% to 69.7% and from 15.8% to 31.2%. This higher utilization reflects less dumped heat rather than more useful heat recovery. The results show that price-driven scheduling reduces both the operating cost and the waste heat dumped by MGT-based microgrids.

Keywords: microgrid; micro gas turbine; ground-source heat pump; day-ahead scheduling; waste heat recovery

Check for updates

Academic Editor: Ali Razban

Received: 22 September 2026
Revised: 30 October 2026
Accepted: 3 November 2026
Published: 6 November 2026

Copyright: © 2026 by the authors. Licensee MDPI, Basel, Switzerland. This article is an open access article distributed under the terms and conditions of the Creative Commons Attribution (CC BY) license.

1. Introduction

The global pursuit of net-zero emissions by 2050 is driving a profound transformation of energy systems worldwide [1]. This transition demands innovative approaches to energy planning, operations, and regulation. Among the key innovations enabling this shift, microgrids stand out for their ability to enhance energy resilience, efficiency, and sustainability. Microgrids are localized energy networks capable of operating independently or in coordination with the main grid. They integrate distributed energy resources, such as photovoltaic panels and wind turbines that convert solar and wind energy, energy storage systems, and combined heat and power (CHP) units. By combining electricity, heat, and gas, microgrids focus on holistic planning and operation, creating a sustainable, reliable, and cost-effective energy ecosystem.

Generating electricity in the range of 3–500 kW and thermal output between 3 and 1500 kW, micro gas turbines (MGTs) achieve overall efficiencies of up to 80%, with exhaust

gas temperatures between 250 and 300 °C [2,3]. MGTs provide a compact, efficient, and flexible solution for CHP applications. Their ability to generate both electricity and heat simultaneously makes them a key technology for decentralized energy systems in residential, commercial, and industrial sectors. Basmadjian et al. [4] conducted an analysis of a microgrid incorporating an MGT and battery storage to supply electricity to a Canadian community. The study employed a Capstone Turbines Corporation C30 MGT with a nominal power of 30 kW, while the battery capacity was optimized to achieve minimal fuel consumption. Das et al. [5] assessed the techno-economic performance of a microgrid integrating photovoltaic (PV) panels, wind turbines, and battery storage, coupled with various prime movers, including diesel generators, MGTs, and fuel cells. The study, conducted across five climatic zones in Australia, found that a microgrid utilizing MGTs achieved the lowest cost of energy across all climates. Kumar et al. [6] explored a microgrid designed to supply electricity, freshwater, and cooking gas to remote areas in India. The system, which included PV panels, battery storage, MGTs, gasifiers, and multi-effect desalination units, produced 80,423 kWh of electricity and 34,779 MJ of heat annually. Furthermore, by utilizing waste heat from the MGTs, the multi-effect desalination units produced 9516 L of freshwater daily.

Over the past few decades, ground-source heat pump (GSHP) systems have gained widespread adoption across Europe, driven by their high energy efficiency and strong backing from renewable energy policies and European Directives [7]. Countries such as France, Germany, Austria, and the Netherlands have seen increasing geothermal heat pump installations, with Scandinavian countries leading the trend [8]. GSHP systems have been implemented in various building types. Miglani et al. [9] analyzed a single-family residential building in Zurich, Switzerland, utilizing a GSHP and solar thermal collector. Through design optimization, they determined an optimal borehole heat exchanger (BHE) length of 160 m, corresponding to a solar collector area of 50 m^2. Hu et al. [10] investigated a five-story office building with a height of 19.2 m and a total conditioned area of 2852 m^2. The building's heating and cooling demands are met by two GSHPs coupled with a 40 m^3 water storage tank. The nominal cooling and heating capacities of the heat pumps are 88 kW and 72 kW, respectively. Figueira et al. [11] introduced a GSHP system implemented in a resort in Portugal, designed to meet a heating demand of 2370 kW and a cooling demand of 1100 kW. The system also supplies domestic hot water and supports swimming pool heating. To achieve this, four groups of BHEs were installed: 40 boreholes at a depth of 100 m, 60 at 125 m, and two separate clusters of 72 at 115 m.

Day-ahead load scheduling is a widely adopted approach to optimize microgrid operations. It involves planning and optimizing energy generation and consumption for the next 24 h. The process determines the optimal operation of energy supply units, such as diesel generators, MGTs, and renewable sources, and manages the charging and discharging of storage units to meet electricity, heating, or cooling demands at the lowest operational cost or other specified objectives. It also allows the microgrid to participate in electricity markets, buying or selling power based on its needs and market conditions. Zhang et al. [12] presented a day-ahead load scheduling for a microgrid with PV panels, wind turbines, batteries, thermal energy storage units, and MGTs. The objective was to minimize daily operating costs while ensuring operational constraints and load balance were satisfied. In [13], day-ahead load scheduling was applied to a microgrid comprising PV panels, wind turbines, fuel cells, MGTs, and batteries. The scheduling strategy was implemented for four typical days representing different seasons. A modified krill herd optimization algorithm was proposed to minimize the total operating cost over the scheduling period. Chen et al. [14] proposed a day-ahead load scheduling approach for a residential building equipped with PV systems, electric vehicle chargers, air conditioners, and other appliances. The scheduling

was implemented in two scenarios: working days and weekends. The approach successfully shifted peak load to off-peak times, reduced electricity bills, and maintained the comfort of occupants.

Established modeling platforms have also been applied to the day-ahead scheduling problem. Santos et al. [15] coupled the MATLAB Link module of HOMER Pro 2020 (Hybrid Optimization of Multiple Energy Resources) with an AMPL-based mixed-integer linear programming model to determine the day-ahead operation of a grid-connected campus microgrid comprising PV generation, battery storage, and grid exchange, and reported economic advantages over the default dispatch strategies provided by HOMER. Milan et al. [16] applied the DER-CAM (Distributed Energy Resources Customer Adoption Model) platform to the operation scheduling of CHP-based distributed energy systems, determining the optimal dispatch of generation and storage units within a mixed-integer linear programming framework that minimizes total energy costs.

From the review of published studies, key research gaps have been identified as follows:

- Fluctuating energy demands often force MGTs to operate under off-design conditions, representing a substantial portion of their total operation time. While most existing studies [4–6] on the operation optimization of MGTs within microgrids use simplified models to improve computational efficiency, these models often overlook the off-design performance of MGTs. This simplification leads to discrepancies between the simulated and actual performance of MGTs under real-world operational conditions. The same limitation applies to the established platforms discussed above [15,16]; neither representation captures the continuous dependence of MGT fuel consumption and exhaust gas temperature on part-load ratio and ambient conditions, which is precisely the off-design behavior that governs the operating cost of the MGT-based microgrid under fluctuating demand.
- Both GSHPs and MGTs are commonly used in microgrid applications, but their integration has not been sufficiently studied. Only a limited number of studies, such as [17] and [18], have explored the sizing of this combined configuration. However, the operation optimization of this integrated configuration, which could enhance the energy efficiency of microgrids, remains an underexplored area.

To address these gaps, this paper presents a day-ahead operation optimization of a microgrid integrating an MGT, a GSHP, and a PV system to meet the electricity and heating demands of office buildings, represented by the U.S. Department of Energy Medium Office prototype building model rather than a specific existing building. The building and its demand are described inSection 2. The main contributions of this work are summarized as follows:

- A validated data-driven MGT model, based on a feedforward neural network trained on measured Ansaldo Energia T100 operating data, is embedded directly in the scheduling problem. Fuel consumption and exhaust gas temperature are therefore predicted as continuous functions of part-load ratio and ambient conditions, so that the off-design performance of the MGT is retained rather than approximated by the constant or linear efficiency curves.
- The MGT, GSHP, and PV models are integrated into a dynamic Modelica model of the microgrid, in which the electrical and thermal sides are explicitly coupled through the electricity consumption of the GSHP and the recovery of MGT waste heat. The combined MGT-GSHP configuration, whose operation optimization has so far received limited attention, is thereby addressed.
- A genetic algorithm is employed to determine the hourly capacity and on-off status of the MGT over a 24-h horizon, using day-ahead electricity prices to minimize the total operating cost of the microgrid.

- The optimized dispatch is compared against a rule-based control strategy for two representative operating conditions, contrasting a high heating demand case with a low heating demand case. The resulting differences in operating cost, electrical dispatch pattern, and waste heat utilization are quantified for both strategies.

2. System Description

This study examines a microgrid integrating MGT, PV system, and GSHP to meet both the electricity and heating demands of office buildings. Electricity is supplied by the PV system, the MGT, and the grid, which together serve the building's electrical loads and the GSHP. Heating is provided by the waste heat recovered from the MGT together with the heat delivered by the GSHP. Since the GSHP is electrically driven, its power consumption adds to the electrical load that these sources must meet, thereby coupling the electrical and thermal sides of the system. Figure 1 shows the schematic of the microgrid. The main specifications of the microgrid components used in the case study are summarized in Table 1.

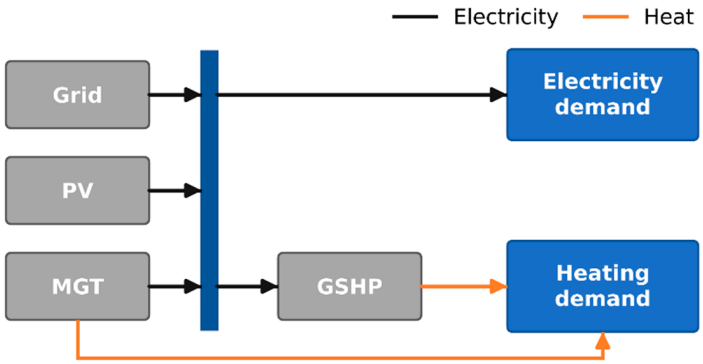


Figure 1. Schematic of the microgrid.

Table 1. Specifications of the microgrid components in the case study.

Component	Parameter	Value
MGT	Model/fuel	Ansaldo Energia T100/biogas
	Electrical output range	60–110 kW
PV array	Module type	Q.PLUS BFR-G4.1 285 W
	Number of modules	700
	Rated capacity	199.5 kWp
Heat pump	Model	WaterFurnace NKW130
	Rated heating capacity	172 kW
	COP	4
BHE field	Number of boreholes	10
	Borehole depth/spacing	70 m/2 m
	Borehole type	Double U-tube (DN32)
	Working fluid	Water–ethanol (25%)
	Ground thermal conductivity/capacity	2.8 W/(m·K)/2.1 × 10^6 J/(m^3·K)
	Grout thermal conductivity	1.5 W/(m·K)
	Undisturbed ground temperature	8 °C

The electricity and heating demand profiles of the office building were generated with EnergyPlus [19]. Two U.S. Department of Energy prototype Medium Office buildings [20] were simulated under the weather conditions of Stavanger, Norway. The U.S. Department of Energy prototype building models, developed by the Pacific Northwest National Laboratory, are a publicly available set of EnergyPlus models representing the principal commercial

building types, and are widely used as standardized load profiles in building energy studies. They were adopted in this study because they provide complete and publicly documented building descriptions, which makes the load profiles reproducible. To the authors' knowledge, no comparable open, simulation-ready reference model of a Norwegian or European office building is currently available. The Medium Office prototype adopted here represents a three-story office building with a floor area of 4982 m^2, giving 9964 m^2 for the two buildings considered. The model specifies the building geometry, envelope constructions, internal loads from occupants, lighting and equipment, operating schedules and the HVAC system. These inputs were used without modification, and only the weather file was replaced with Stavanger data. The hourly electricity and heating demand profiles used in this study are therefore simulation results rather than measured data. The weather data are taken from the International Weather for Energy Calculations (IWEC) Stavanger–Sola file, which represents typical long-term conditions rather than a single measured year. The simulation generates hourly electricity and heating demand profiles, which represent the load that the microgrid must satisfy over the operating period. The simulation is run for a full year, so that the seasonal variation in both demands is captured. The heating demand is strongly seasonal, with the monthly heating demand falling from 95 MWh in winter to 1.9 MWh in summer, whereas the non-heating electricity demand remains nearly constant throughout the year. From this annual profile, two representative days were selected for the scheduling study: one with high heating demand (Case 1) and one with low heating demand (Case 2). It should be noted that the electricity demand considered here includes only the non-heating electrical loads, such as lighting, interior equipment, office appliances, and ventilation fans, and excludes any electricity used for space heating. The heating demand is met by the GSHP together with the waste heat recovered from the MGT. The electricity consumed by the GSHP to provide this heat is therefore not included in the building electricity demand; it is added to the total microgrid electricity demand, as illustrated in Figure 1.

Two representative days are considered to capture the contrast in building load profile. They were selected from the annual simulation as working days, when the office building is occupied, with clearly different heating demand but a similar non-heating electricity demand, so that the comparison isolates the effect of the heating demand on the scheduling. Case 1 corresponds to 2 January, a day in the heating season with a daily heating demand of 1355 kWh. On this day, a large part of the heat recoverable from the MGT exhaust can be used in the building. Case 2 corresponds to 21 November, with a daily heating demand of 461 kWh. On this day, the recoverable waste heat largely exceeds the heating demand. The corresponding hourly electricity and heating demand profiles for the two cases are presented in Figure 2.

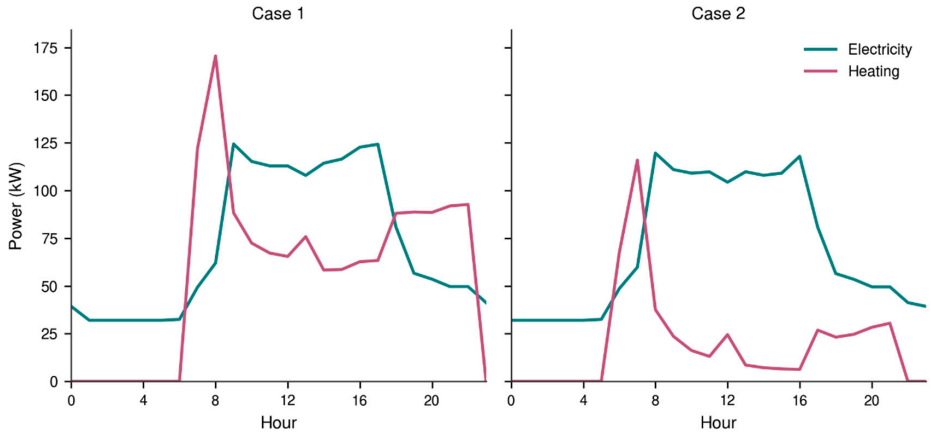


Figure 2. Electricity and heating demand profiles for two cases.

3. Modeling and Validation

The dynamic behaviors of microgrids are explored in this research through the use of Modelica, an object-oriented, equation-based programming language. There has been considerable contribution from the global Modelica community in producing established open-source software packages that are essential for simulating and modeling microgrids and energy systems in buildings.

3.1. Micro Gas Turbine

Evaluating the off-design performance of MGTs is a challenging task. Typically, detailed thermodynamic models are used to evaluate their performance under varying operational and environmental conditions. However, these models are computationally expensive, hindering their use for day-ahead load scheduling. To tackle this issue, this paper utilizes a validated data-driven MGT model that leverages real-world operational data to achieve fast and accurate predictions. The model is built using an artificial neural network, specifically a feedforward neural network (FFNN), where data flows sequentially from input to output layers. The model considers four input variables: ambient temperature, ambient pressure, air humidity, and power demand, and predicts two outputs: fuel consumption and exhaust gas temperature. The FFNN architecture features three hidden layers, with exponential linear unit (ELU) and rectified linear unit (ReLU) as activation functions. The mean squared error (MSE) is used as the cost function, and the adaptive gradient algorithm (AdaGrad) is chosen as the optimizer. Detailed hyperparameter settings can be found in our previous publication [18].

The data-driven model was developed using operational data from an Ansaldo Energia T100 recorded over a range of ambient conditions and power outputs [18]. The dataset was split randomly into 70% for training, 10% for validation and 20% for testing, and the test data were excluded from the training process [18]. Figure 3 compares the measured fuel consumption and exhaust gas temperature with the predictions of the model on the test data. The model follows the step changes in power output, with fuel consumption varying between approximately 5 and 7.6 g/s and exhaust gas temperature between approximately 230 and 270 °C. The resulting mean absolute percentage error (MAPE) is 0.25% for fuel consumption and 0.19% for exhaust gas temperature [18]. Because consecutive samples of operational data are strongly correlated, a random split mainly reflects the accuracy of the model within the recorded operating conditions and may overstate its accuracy for new conditions. The model is therefore applied only within the ambient and load range covered by its training data. For a more detailed description of the modeling and validation of the MGT, please refer to our previous publication [18].

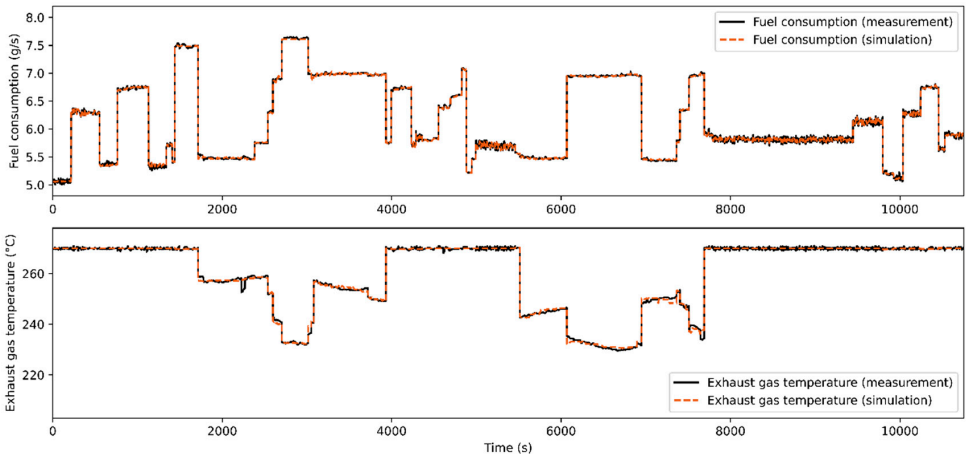


Figure 3. Validation of data-driven MGT model.

3.2. Ground-Source Heat Pump

The BHE and the brine-to-water heat pump are fundamental components of a GSHP system. The BHE consists of vertical boreholes filled with a circulating water-antifreeze solution that extracts heat from the ground in winter and releases it back during summer. The brine-to-water heat pump then moves this energy to or from the building, providing efficient year-round heating and cooling.

The BHE model is developed using the MoBTES package [21] in Modelica, incorporating the thermal resistance and capacity model (TRCM) to enhance short-term heat transfer accuracy within the borehole. The heat exchange with the surrounding ground is modeled using the finite difference method. Model validation is performed using operational data from the Universitat Politècnica de València (UPV) in Spain [22]. The BHE configuration consists of six single U-tube boreholes arranged in a parallel layout, each measuring 50 m in depth with a spacing of 3 m. Detailed specifications are provided in Table 2.

Table 2. Specifications of the BHE at the UPV, Spain.

Parameter	Value
Working fluid	Water
Tube outer diameter	0.016 m
Tube inner diameter	0.0127 m
Tube shank spacing	0.07 m
Borehole depth	50 m
Borehole diameter	0.150 m
Borehole number	6
Borehole distance	3 m
Pipe thermal capacity	1.81×10^6 J/(m^3·K)
Pipe thermal conductivity	0.4 W/(m·K)
Grout thermal capacity	3.2×10^6 J/(m^3·K)
Grout thermal conductivity	2.09 W/(m·K)
Ground thermal capacity	3.2×10^6 J/(m^3·K)
Ground thermal conductivity	2.09 W/(m·K)

The model was validated against field measurements collected over four days, from 13 to 16 September 2005, while the GSHP operated in cooling mode. As shown in Figure 4, the BHE inlet temperature and flow rate were used as boundary conditions. Model accuracy was evaluated by comparing the simulated and measured outlet temperatures of the BHE, which agree well over the entire operation period. Although small deviations occur during the off periods, they do not influence the calculated heating capacity or energy consumption. After removing the off periods, the comparison gives a low MAPE of 2.81%.

The validation above covers four days of operation in cooling mode. To assess the long-term predictive capability of the BHE model, including heat extraction from the ground, the model was validated in our previous work [18] against one year of operational data from the borehole thermal energy storage (BTES) system in Brædstrup, Denmark. The system supplies heat to approximately 1500 households and stores excess heat from 18,600 m^2 of solar thermal collectors in a field of 48 double U-tube boreholes with a depth of 45 m and a spacing of 3 m. The parameters of the bore field are listed in Table 3. The measured volume flow rate and inlet temperature were applied as boundary conditions, and the simulated outlet temperature of the working fluid was compared with the measured value. The selected year comprises a charging period during the first 3217 h, with inlet temperatures between 45 and 85 °C, and a discharging period from 3527 h to 7861 h, during which heat was extracted from the ground at inlet temperatures between 10 and 25 °C. Periods with zero flow rate, during which the BTES was not in operation, were excluded

from the comparison. As shown in Figure 5, the model reproduced the measured outlet temperature with a MAPE of 2.27% over the full year [18]. The discharging period, which covers approximately 4300 h of heat extraction, is particularly relevant for the heating-dominated operation considered in this study, as it confirms that the model captures the ground response during extended heat extraction. The bore-field configurations in Tables 2 and 3 were used only for model validation; the bore field and heat pump of the investigated microgrid are specified in Table 1.

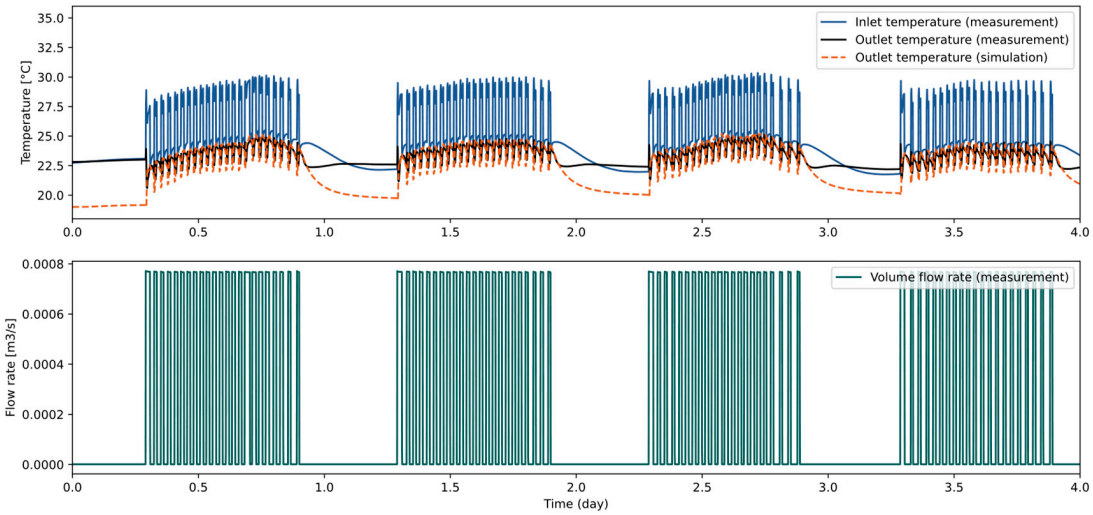


Figure 4. Validation of the BHE model with four days of operational data at the UPV.

Table 3. Specifications of the BTES in Brædstrup, Denmark [18].

Parameter	Value
Working fluid	Water
Tube outer diameter	0.032 m
Tube inner diameter	0.0262 m
Tube shank spacing	0.088 m
Borehole depth	45 m
Borehole diameter	0.150 m
Borehole number	48
Borehole distance	3 m
Pipe thermal capacity	1.5×10^6 J/(m^3·K)
Pipe thermal conductivity	0.4 W/(m·K)
Grout thermal capacity	3×10^6 J/(m^3·K)
Grout thermal conductivity	1.44 W/(m·K)
Ground thermal capacity	1.96×10^6 J/(m^3·K)
Ground thermal conductivity	1.72 W/(m·K)

The ground was initialized at an undisturbed temperature of 8 °C, representative of the Stavanger region. To account for the thermal history of the bore field, each case day was preceded by a one-year simulation of the GSHP operation using the annual heating demand profile, so that the ground and brine temperatures at the start of the case day reflect the preceding heat extraction.

A regression model developed from a manufacturer's catalog is utilized to simulate the brine-to-water heat pump [23]. The model uses inputs such as the source-side brine inlet temperature, brine flow rate, load-side water inlet temperature, and water flow rate to estimate power consumption and heating capacity. Validation was conducted using the catalog data of the WaterFurnace NKW130 heat pump, which is the same model as that

used in the case study (Table 1), and the results, presented in Figures 6 and 7, show close agreement with catalog data, with relative errors under 5% for both heating capacity and power consumption. Additional information can be found in our earlier publication [18].

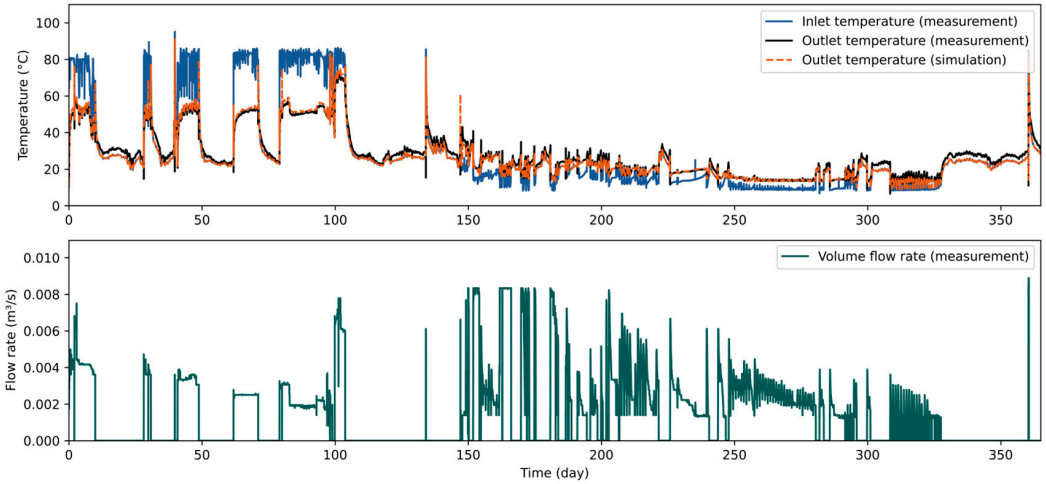


Figure 5. Validation of the BHE model with one year of operational data from the BTES in Brædstrup, Denmark (results previously reported in [18]).

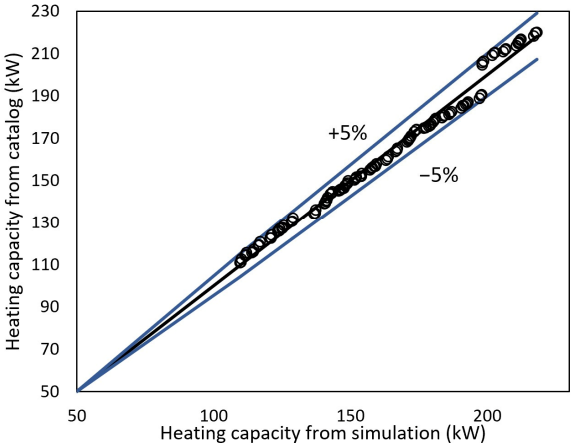


Figure 6. Validation of heat pump's heating capacity.

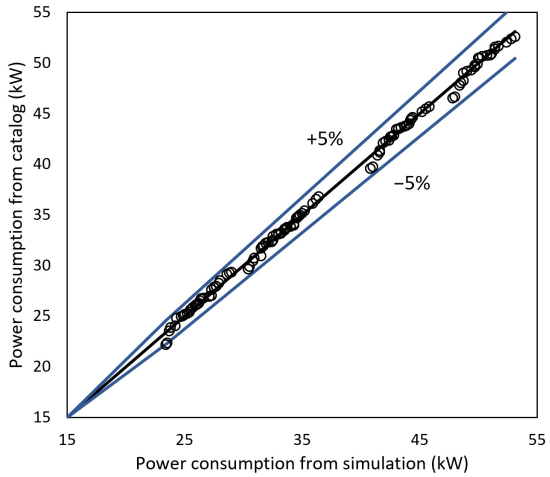


Figure 7. Validation of heat pump's power consumption.

3.3. Solar PV Panel

To capture the nonlinear electrical behavior of the PV panel under fluctuating cell temperatures and solar irradiance, the open-source Modelica package AixLib is utilized. The PV cell's characteristics are defined using the Single-Diode method [24], while an empirical model estimates cell temperature based on the panel's mounting configuration.

Operational data from a rooftop PV system at the National Institute of Standards and Technology (NIST) campus, comprising 312 Sharp NU-U235F2 modules with a total rated capacity of 73.3 kW, is used to validate the PV panel model's accuracy [25]. Data collected between June 6 and June 13, 2016, are used to evaluate the model's ability to predict power generation, considering key influencing factors such as solar irradiance, wind speed, and ambient temperature. As illustrated in Figure 8, the model closely aligns with actual performance, achieving a MAPE of 6%.

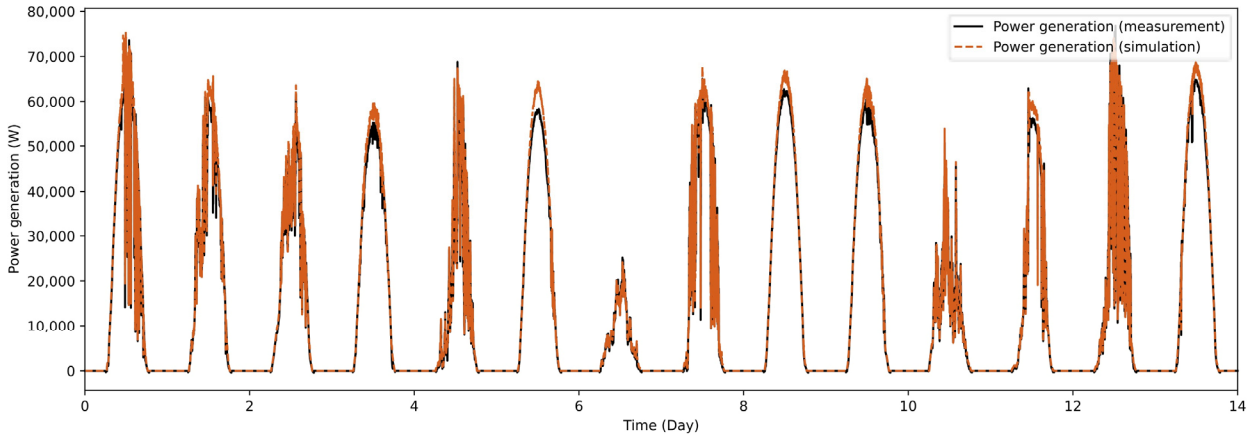


Figure 8. Validation of PV power generation.

3.4. Operation Strategies

To evaluate the benefit of coordinated microgrid operation, two control strategies are implemented and compared: a rule-based strategy and a day-ahead optimization strategy, which schedules the MGT, GSHP, and grid import for the next 24 h based on electricity prices. Both strategies operate on the same validated component models described above, the data-driven MGT model, the GSHP model, and the PV model, ensuring a consistent basis for comparison. The overall calculation process, from the input data to the comparison of the two strategies, is illustrated in Figure 9.

The rule-based strategy applies a fixed priority order. Electrical demand is served first by PV generation, then by the MGT when PV output is insufficient, with any remaining deficit imported from the grid. On the thermal side, heating demand is met first by MGT waste heat whenever the MGT is running; if this is insufficient to cover the load, the GSHP supplies the remaining heat. When the MGT is off, the GSHP alone meets the full heating demand.

The day-ahead optimization strategy formulates the scheduling problem to minimize total daily operating cost, comprising the cost of grid electricity import, which includes the electricity consumed by the GSHP, and the MGT fuel cost, subject to hourly electrical and thermal balance constraints. The optimization is carried out using the Dymola optimization package, which supports multiple optimization algorithms. A genetic algorithm is selected here because it treats the Modelica model as a black box and evaluates each candidate schedule over the full 24-h horizon, including the dynamic response of the bore field, without requiring the problem to be reformulated. The same approach can be extended

directly to include start-up costs, minimum up- and down-times or thermal energy storage, which couple consecutive hours more strongly.

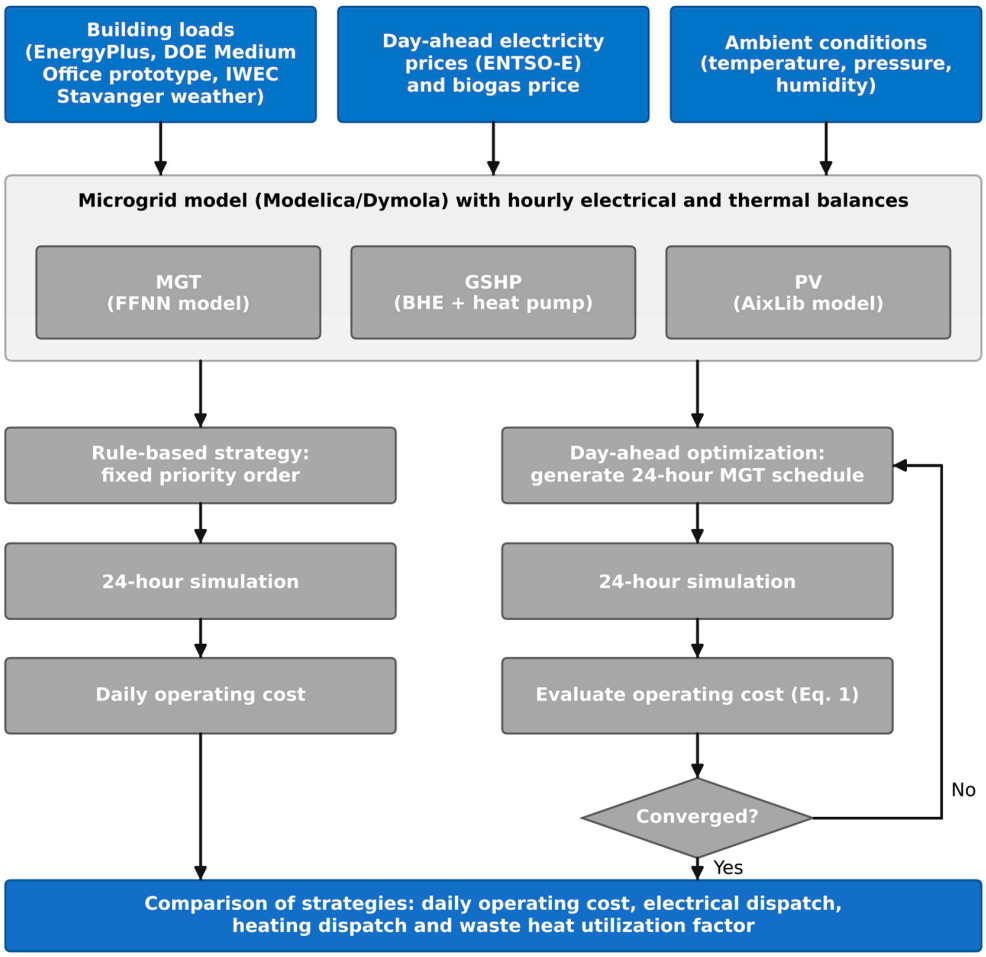


Figure 9. Workflow of the day-ahead operation optimization and the rule-based strategy.

The genetic algorithm of the Dymola Optimization library was used with a population size of 10 and 100 generations, corresponding to 1000 model evaluations per case. The algorithm operates as a micro-genetic algorithm with elitism, niching and up to 100 restarts, using a crossover probability of 0.5, a mutation probability of 0.02 and a creep mutation probability of 0.04, which are the default settings of the library. The search is started from an initial set-point of 75 kW for all 24 h, and the further individuals of the population are generated by the algorithm within the bounds of the set-points. The optimization terminates after the specified number of generations. The random seed is fixed in the library and cannot be changed by the user, so a repeated run with the same setup reproduces the reported solution exactly, and independent runs with different seeds are not possible.

The optimization objective can be represented as follows:

$$Cost = \int_{t=0}^{t=24} \left[P_{grid}(t) \cdot c_e(t) + \dot{Q}_{fuel}(t) \cdot c_g \right] dt \quad (1)$$

where

Cost—Operation cost of the microgrid (NOK);
P_{grid}—Power imported from the grid, including the electricity consumed by the GSHP (kW);
c_e—Hourly day-ahead electricity price (NOK/kWh);
$\dot{Q}_{fuel}$—Fuel energy input rate of the MGT (kW);
c_g—Price of biogas (NOK/kWh);

t—Time (h).

The fuel energy input rate of the MGT is calculated from the fuel mass flow rate predicted by the data-driven model. Since the electricity consumed by the GSHP is part of the electrical balance in Equation (5), it is included in the grid import whenever it is not covered by PV or the MGT, and it is not counted as a separate cost term.

The decision variables of the optimization are the hourly power set-points of the MGT, $u(t)$, for the 24 h of the scheduling horizon. Each set-point is held constant over its hour. The MGT is either switched off or operated within its permissible load range:

$$P_{MGT}(t) \in \{0\} \cup [60, 110] \text{ kW} \tag{2}$$

The commitment of the MGT is represented by a binary variable, which distinguishes shutdown from operation at or above the minimum load. Instead of being optimized as a separate variable, it is derived from the set-point, which the genetic algorithm treats as a continuous variable. The MGT is switched off when the set-point is below the minimum load of 60 kW or exceeds the net electricity demand of the building and the GSHP, i.e., after subtracting the PV generation. The on/off status $\delta(t)$ and the power output of the MGT, $P_{MGT}(t)$, are therefore:

$$\delta(t) = \begin{cases} 1, & 60 \text{ kW} \le u(t) \le P_{\text{load}}(t) + P_{\text{GSHP}}(t) - P_{\text{PV}}(t) \\ 0, & \text{otherwise} \end{cases} \tag{3}$$

$$P_{MGT}(t) = \delta(t) \cdot u(t) \tag{4}$$

When the MGT is switched off, its fuel consumption and recoverable waste heat are zero. The electricity demand of the building and the electricity consumption of the GSHP are met by PV generation, the MGT and grid import. Electricity export to the grid is not allowed, so the hourly electrical balance is:

$$P_{PV}(t) + P_{MGT}(t) + P_{grid}(t) = P_{load}(t) + P_{GSHP}(t), P_{grid}(t) \ge 0 \tag{5}$$

where P_{PV}, P_{grid}, P_{load} and P_{GSHP} are the PV power generation, the grid import, the electricity demand of the building and the electricity consumption of the GSHP, respectively. If the set-point exceeds the net electricity demand of the building and the GSHP, the MGT is switched off for that hour, and the demand is covered by PV generation and grid import. Grid import is not limited by a connection capacity. The model uses aggregate hourly energy balances. Network constraints, such as voltage, reactive power and protection, are not modeled. These are addressed in dedicated studies [26,27]. In the two cases studied, PV generation is low and never exceeds the remaining demand, so no surplus electricity arises and neither curtailment nor export is required. On the thermal side, the heating demand is covered first by the recovered MGT waste heat and then by the GSHP, and excess waste heat is dumped, as defined by Equations (8)–(10) in Section 3.5. The heat output of the GSHP is limited by its rated heating capacity of 172 kW (Table 1). Since the peak heating demand is approximately 145 kW, the GSHP can cover the full heating demand when the MGT is switched off, and this limit is not reached in either case. Given the set-points $u(t)$, the Modelica model calculates the MGT fuel consumption and exhaust conditions with the data-driven model, as well as the PV output, the GSHP electricity consumption and the grid import for each hour. The balances are therefore satisfied by the simulation model itself, with grid import and GSHP output covering the remaining electrical and heating demand, so the genetic algorithm only has to handle the bounds of the set-points and no penalty terms are required. Because every set-point corresponds to a feasible operating state, all individuals generated by the genetic algorithm are feasible, and no constraint violations occur. The MGT is switched off at the start of the scheduling horizon. Since neither start-up

costs nor minimum up- and down-times are considered, the initial state of the MGT does not affect the schedule, and consecutive hours are coupled only through the thermal state of the bore field. The initialization of the ground temperature is described in Section 3.2.

The hourly day-ahead electricity price profiles used in the optimization are shown in Figure 10, with Case 1 shown on the left and Case 2 shown on the right. Prices are reported in NOK/kWh for each hour of the day. Data were obtained from the European Network of Transmission System Operators for Electricity (ENTSO-E) Transparency Platform [28]. The prices correspond to the bidding zone NO2 (Southwest Norway), in which Stavanger is located, for the same calendar dates as the load profiles in 2025, i.e., 2 January 2025 for Case 1 and 21 November 2025 for Case 2. Since the load profiles are based on typical weather data, the load and price profiles are matched by date but do not originate from the same year. The two price profiles also differ in shape: the price in Case 1 shows a broad daytime plateau, whereas the price in Case 2 shows a sharp morning peak followed by a steady decline. The MGT is fueled by biogas; the fuel price of 0.18 NOK/kWh is based on information provided by Lyse Energi AS, the local energy supplier in Stavanger [29]. Unlike electricity, biogas is not traded on an hourly market, so the fuel price is held constant over the 24-h scheduling horizon.

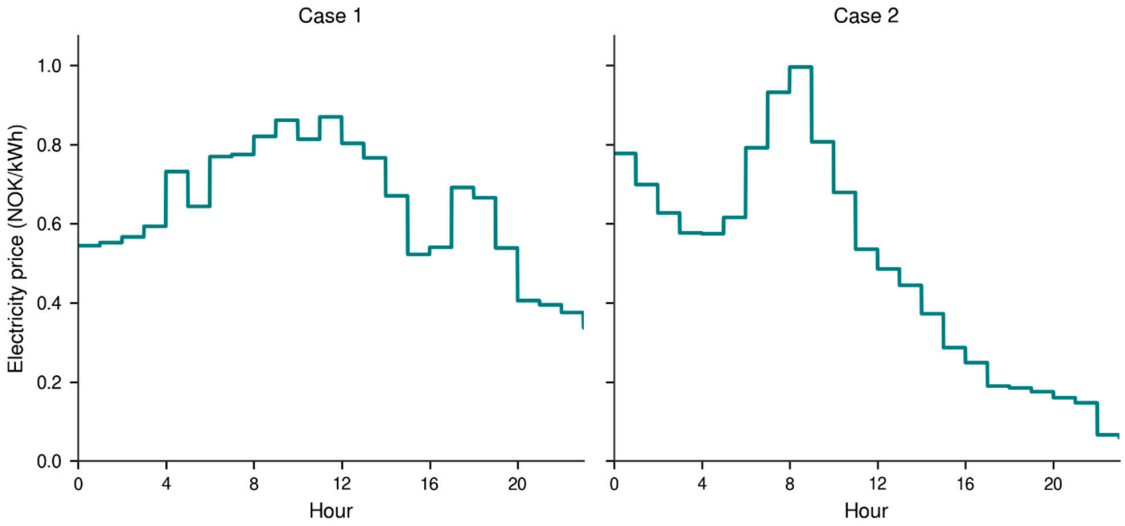


Figure 10. Day-ahead electricity price profiles.

3.5. Waste Heat Recovery and Utilization Factor

The heat recovered from the MGT exhaust is calculated from the exhaust gas temperature, which is predicted by the data-driven model, and the exhaust gas mass flow rate, which is calculated as the sum of the combustion air and fuel mass flow rates:

$$\dot{m}_{exh}(t) = \dot{m}_{air}(t) + \dot{m}_{fuel}(t) \tag{6}$$

where $\dot{m}_{fuel}$ is the fuel consumption predicted by the data-driven model and $\dot{m}_{air}$ is approximated as proportional to the electrical output, increasing linearly from zero to 0.88 kg/s at the maximum output of 110 kW. The recoverable heat is then:

$$\dot{Q}_{avail}(t) = \dot{m}_{exh}(t) \cdot c_{p,exh} \cdot (T_{exh}(t) - T_{exh,out}) \tag{7}$$

The exhaust gas is assumed to have a specific heat capacity of 1.1 kJ/(kg·K), evaluated at the mean temperature of the exhaust gas in the heat recovery unit and treated as constant. The exhaust outlet temperature of the heat recovery unit is set to 110 °C, chosen to remain above the acid dew point of the combustion products and thereby avoid condensation and

corrosion in the heat exchanger. When the MGT is switched off, the fuel and exhaust gas mass flow rates, and thus the recoverable heat, are zero.

Equation (7) represents the recoverable heat under the assumption of ideal heat transfer without thermal losses in the heat recovery unit. These relations were checked against the manufacturer's data at nominal load. At an electrical output of 100 kW, the model yields an exhaust mass flow rate of 0.805 kg/s and an exhaust temperature of approximately 270 °C, in agreement with the specified values of approximately 0.79 kg/s and 270 °C. The resulting recoverable heat of approximately 142 kW is lower than the rated thermal output of 165 kW, because the outlet temperature of 110 °C assumed in this study is higher than that of the manufacturer's heat recovery unit. The waste heat estimate is therefore conservative. The exhaust gas leaves the recuperator of the MGT at approximately 270 °C, which is well above the supply temperature of the building heating system. The recovered heat can therefore be delivered at the required temperature, and the delivery temperature does not limit the heat recovery.

Because the heat recovery unit cannot store energy, only the portion of the available heat that coincides with an instantaneous heating requirement can be delivered to the building. The usefully recovered heat is therefore limited by the heating demand:

$$\dot{Q}_{used}(t) = min(\dot{Q}_{avail}(t), \dot{Q}_{dem}(t)) \quad (8)$$

and the remaining exhaust energy is dumped to ambient:

$$\dot{Q}_{dump}(t) = \dot{Q}_{avail}(t) - \dot{Q}_{used}(t) \quad (9)$$

The residual heating demand not covered by the MGT is supplied by the GSHP:

$$\dot{Q}_{GSHP}(t) = \dot{Q}_{dem}(t) - \dot{Q}_{used}(t) \quad (10)$$

The corresponding daily energy quantities reported in Section 4.2.3 are obtained by integrating each heat rate over the 24-h scheduling horizon:

$$Q_i = \int_{t=0}^{t=24} \dot{Q}_i dt \quad (11)$$

where the subscript i denotes any of the four heat flows defined above. The waste heat utilization factor is then defined as the fraction of the recoverable exhaust heat that is usefully employed over the day:

$$\eta_{rec} = \frac{\int_{t=0}^{t=24} \dot{Q}_{used} dt}{\int_{t=0}^{t=24} \dot{Q}_{avail} dt} \quad (12)$$

where

Q_{avail}—Recoverable exhaust heat of the MGT (kWh);
$\dot{m}_{exh}$—Exhaust gas mass flow rate (kg/s);
$\dot{m}_{air}$—Combustion air mass flow rate (kg/s);
$\dot{m}_{fuel}$—Fuel mass flow rate (kg/s);
$c_{p,exh}$—Specific heat capacity of the exhaust gas (kJ/(kg·K));
T_{exh}—Exhaust gas temperature (°C);
$T_{exh,out}$ —Outlet temperature of the heat recovery unit (°C);
Q_{used}—Usefully recovered heat (kWh);
Q_{dem}—Heating demand of the building (kWh);
Q_{dump}—Heat rejected to ambient (kWh);
Q_{GSHP}—Heat supplied by the GSHP (kWh);
Q_i—Daily energy of heat flow i (kWh);
η_{rec}—Waste heat utilization factor (-).

4. Results and Discussion

4.1. Electricity Dispatch Under Rule-Based and Day-Ahead Optimized Operation

To evaluate the benefit of day-ahead optimization over rule-based control, the hourly electrical dispatch is compared for two representative operating conditions: Case 1 and Case 2. Figures 11 and 12 show the results for Case 1 under rule-based and optimized operation, while Figures 13 and 14 provide the corresponding comparison for Case 2. The comparison illustrates how the two strategies allocate PV generation, MGT output, and grid imports to meet the electricity demand under contrasting operating conditions.

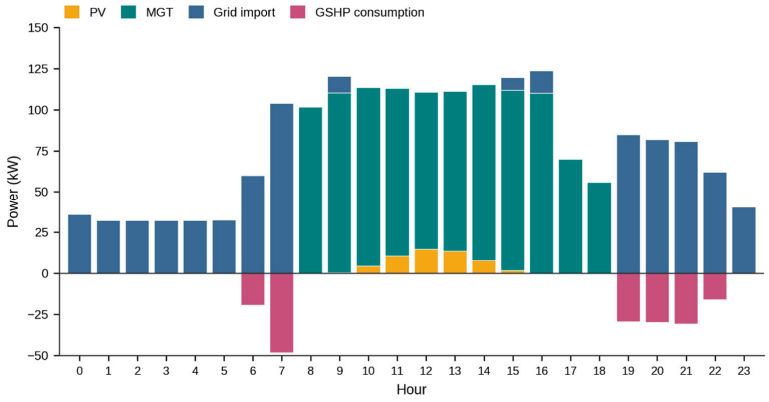


Figure 11. Electricity dispatch under rule-based strategy (Case 1).

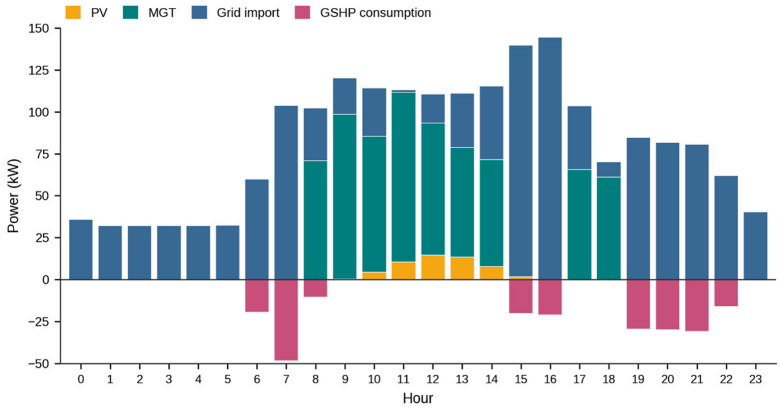


Figure 12. Electricity dispatch under day-ahead optimization (Case 1).

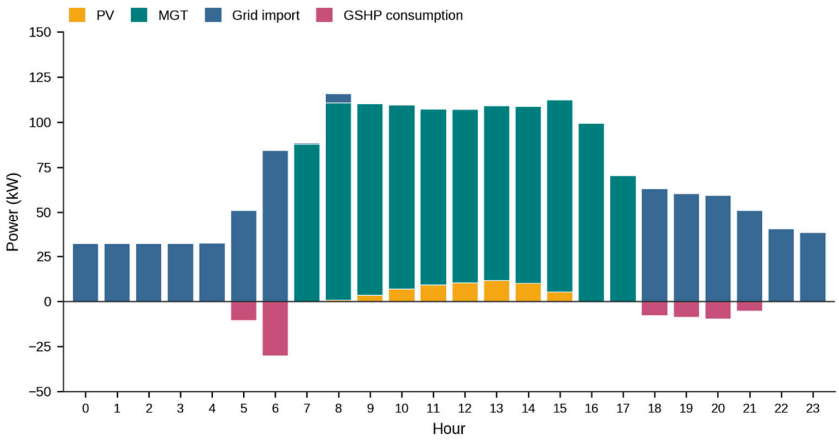


Figure 13. Electricity dispatch under rule-based strategy (Case 2).

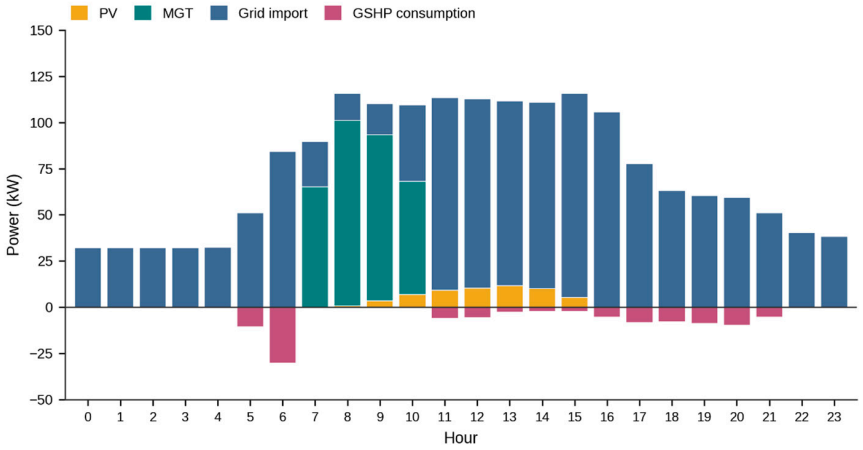


Figure 14. Electricity dispatch under day-ahead optimization (Case 2).

4.1.1. Case 1: Electricity Dispatch

Under rule-based control (Figure 11), the MGT is dispatched whenever PV output is insufficient to cover the electricity demand, without reference to electricity market conditions. This results in continuous operation from 08:00 to 18:00, during which the MGT serves as the dominant generation source and largely displaces grid import; from 08:00 to 14:00 and again from 17:00 to 18:00 the MGT covers essentially the entire residual load, with grid electricity required only in smaller amounts at 09:00 and during 15:00–16:00 when demand exceeds the available MGT output. Outside this window, the microgrid relies entirely on the grid: overnight demand from 00:00 to 07:00 and evening demand from 19:00 to 23:00 are met exclusively by imported electricity. PV generation provides a limited offset to the residual demand between 09:00 and 15:00, peaking around midday. GSHP electricity consumption, shown as the negative segment below the zero axis, appears only in two intervals, during the morning ramp at 06:00–07:00 and again in the evening at 19:00–22:00, both of which coincide with periods when heating is required but no MGT exhaust heat is available. Because the schedule is governed by the predefined rule rather than by price signals, the MGT continues to operate through the mid-afternoon interval in which electricity prices fall to a local minimum, while the low-price overnight hours are covered by grid import purely as a consequence of the rule rather than as a deliberate cost-saving decision.

The day-ahead optimized operation (Figure 12) shows a price-responsive pattern. During the low-price overnight period (00:00–07:00), the MGT remains offline and demand is met entirely by grid import. As prices increase between roughly 08:00 and 14:00, the MGT switches on and remains the primary generation source. It is briefly shut down again at 15:00–16:00, when a local price dip makes grid import the cheaper option, before restarting for 17:00–18:00 as prices rise a second time, then staying off through the evening as prices decline. During the hours the MGT does run, it operates at the output level determined by the optimizer, with grid imports covering any residual demand. In effect, the optimization concentrates MGT operation into the higher-price windows of the day and shuts the unit down during the two lower-price intervals (early morning and mid-afternoon). It is also worth noting that the day-ahead optimization strategy results in a different GSHP utilization pattern compared to the rule-based case: when the MGT is offline, its exhaust heat is unavailable, requiring the GSHP to cover a larger share of the heating demand and drawing additional electricity from the grid. Despite this added electricity draw during MGT-off periods, the optimizer still achieves a lower overall operational cost by concentrating purchases in the cheaper price windows.

4.1.2. Case 2: Electricity Dispatch

Under rule-based control (Figure 13), the MGT operates as a single continuous block from 07:00 to 17:00, covering essentially the whole daytime load. Outside this window the microgrid relies entirely on the grid, with imported electricity meeting the full demand overnight (00:00–06:00) and throughout the evening (18:00–23:00). PV generation provides a partial offset to the residual demand between roughly 08:00 and 15:00, peaking around midday. As in Case 1, the schedule follows the building load rather than market prices: the MGT continues to run through the afternoon hours in which the price declines steadily, while the evening and overnight hours, when prices reach their daily minimum, are served by grid import as a consequence of the rule rather than as a deliberate cost decision. During the hours when the MGT is offline and waste heat recovery is unavailable, the heating demand is met by the GSHP, whose electricity consumption is drawn from the grid and appears as the negative segment below the zero axis at 05:00–06:00 and again at 18:00–21:00.

Under the optimized dispatch (Figure 14), the MGT runs only during a single short window from 07:00 to 10:00, coinciding precisely with the sharp morning peak in the electricity price. Once prices enter their steady decline from late morning onward, the MGT is switched off for the remainder of the day, and the load is met by PV generation between roughly 09:00 and 15:00 together with grid import. Outside the MGT window the microgrid draws entirely on the grid, both overnight (00:00–06:00) and across the whole afternoon and evening (11:00–23:00), when prices fall progressively toward their daily minimum. Compared with the rule-based case (Figure 13), where the MGT runs continuously from 07:00 to 17:00 regardless of the price level, the optimized case operates the MGT for far fewer hours and confines its operation to the single highest-price interval of the day, switching off as soon as prices ease rather than following the building load. As a consequence of this shorter MGT runtime, waste heat is unavailable for a much larger part of the day, and GSHP electricity consumption, visible as the negative segments below the zero axis, extends across the afternoon and evening (11:00–21:00) in addition to the early-morning hours (05:00–06:00).

4.1.3. Operational Cost

The economic consequences of the two operation strategies are summarized in Table 4.

Table 4. Summary of operational performance for rule-based and optimized dispatch.

	Operation Cost (NOK/day)		
	Rule-Based	**Optimized**	**Reduction (%)**
Case 1	2593.8	2257.9	13.0
Case 2	1845.6	1222.6	33.8

In Case 1, day-ahead optimization reduces the daily operational cost from 2593.8 NOK to 2257.9 NOK, a saving of 13%. As shown in Figure 12, the optimizer responds to the price spread across the day: the MGT is kept offline through the night and early morning, when grid electricity sits near its daily minimum and therefore represents the lower-cost option. As prices climb into their extended high-price period, MGT generation becomes economically preferable and output is concentrated accordingly. The MGT is switched off again during the mid-afternoon price dip, when grid import is briefly cheaper, and restarted for the secondary price rise in the early evening before shutting down as prices decline toward the end of the day.

In Case 2, day-ahead optimization reduces the daily operational cost from 1845.6 NOK to 1222.6 NOK, a saving of 33.8%. As shown in Figure 14, the optimizer confines MGT

operation to a single short window (07:00–10:00) aligned with the sharp morning price peak, while PV output and low-cost grid imports cover the remaining demand for the rest of the day. The larger saving in Case 2 arises because the price falls steadily from mid-morning onwards, so the rule-based schedule continues to run the MGT through many hours in which grid import would have cost less than on-site generation.

The optimized schedules also change how often the turbine is started and stopped. In Case 1 the MGT is started twice against once under the rule-based strategy, while the operating time falls from 11 to 9 h; in Case 2 the number of starts is unchanged and the operating time falls from 11 to 4 h. Turbine life is affected both by the accumulated operating hours, through creep and oxidation at high temperature, and by the number of start–stop cycles, through thermal fatigue of the hot-section components and the recuperator. Case 2 reduces both operating time and cycling, whereas Case 1 trades two fewer operating hours against one additional start, so its net effect depends on the relative weight given to each. Since the objective function includes neither a start-up cost nor a minimum up- and down-time constraint, nothing penalizes this additional start. If a cost per start were included, it would affect the two strategies equally in Case 2, where both start the MGT once, so the absolute saving would be unchanged, while the percentage saving would decrease slightly because the cost of the rule-based baseline increases. In Case 1, the optimized schedule includes one additional start, so the reported saving would be reduced by the cost of one start. The reported savings should therefore be regarded as upper estimates for Case 1. Including both constraints, and quantifying the resulting trade-off between operating cost and turbine life, is a natural extension of this work.

4.2. Heating Dispatch Under Rule-Based and Day-Ahead Optimized Operation

The same rule-based and day-ahead optimized strategies are now examined from the thermal side, focusing on how heat demand is met by MGT waste heat recovery, GSHP output, and heat dump across Case 1 and Case 2. Figures 15 and 16 show the heating dispatch for Case 1 under rule-based and optimized operation, while Figures 17 and 18 show the corresponding comparison for Case 2. Because MGT waste heat is determined by the unit's electrical output rather than by the building's heat demand, any recovered heat beyond the instantaneous demand must be dumped, while the GSHP steps in whenever the MGT alone cannot meet the load. To make this over-supply visible at a glance, the heating demand profile is overlaid as a dashed line in each figure, so the bar segment above it can be read directly as heat dump.

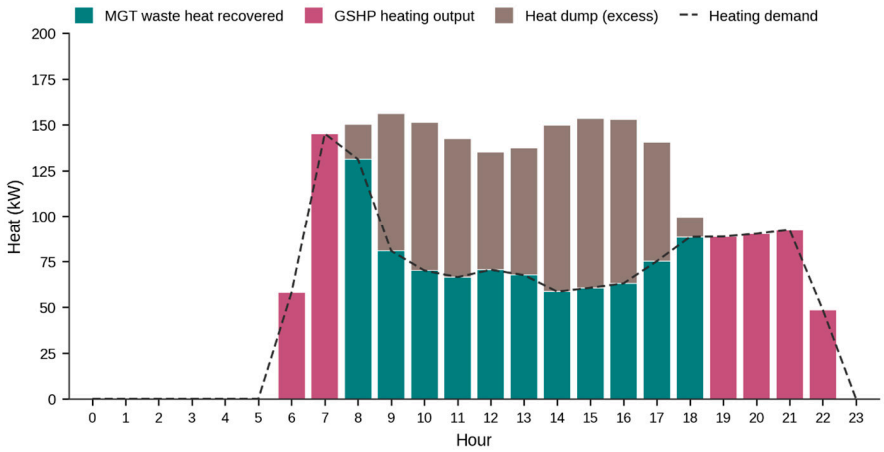


Figure 15. Heating dispatch under rule-based strategy (Case 1).

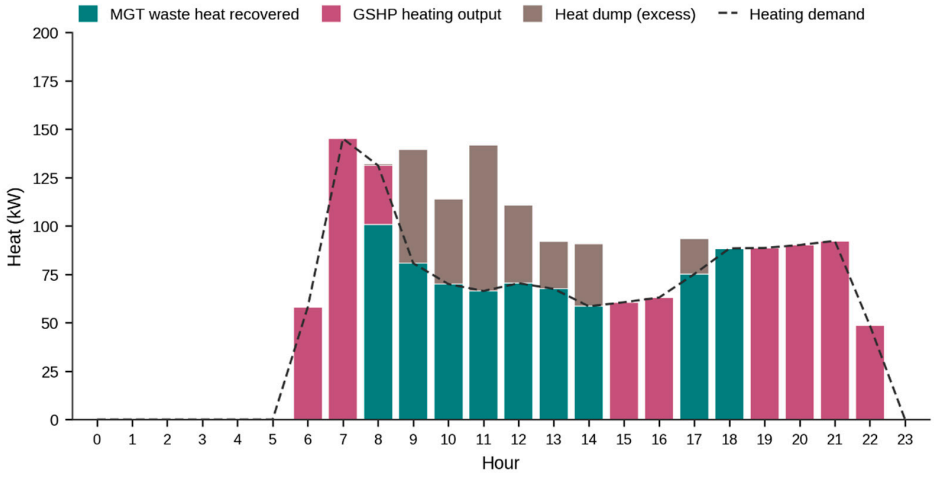


Figure 16. Heating dispatch under day-ahead optimization (Case 1).

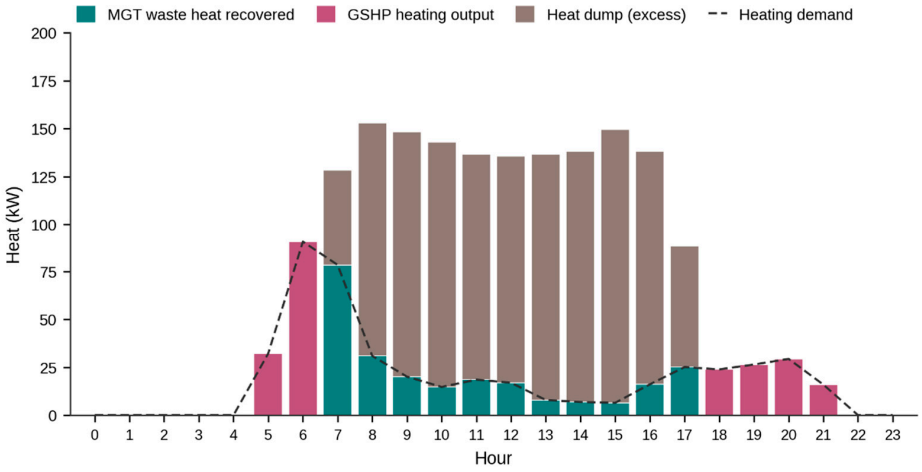


Figure 17. Heating dispatch under rule-based strategy (Case 2).

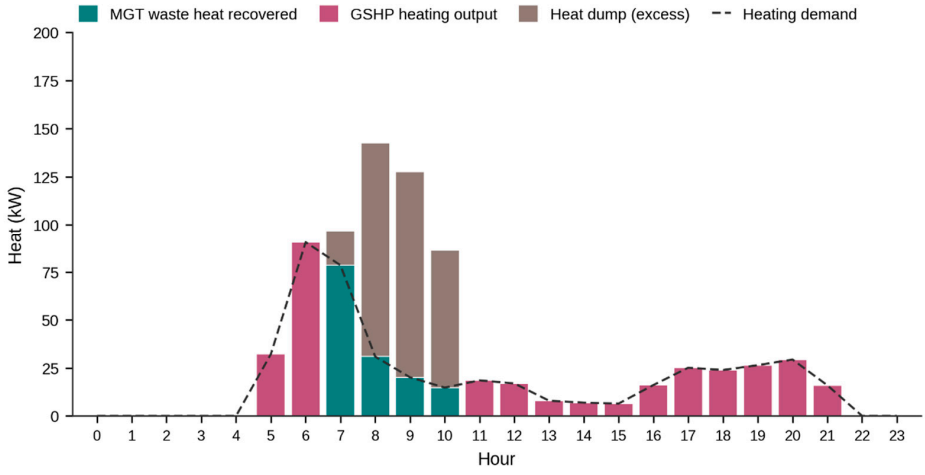


Figure 18. Heating dispatch under day-ahead optimization (Case 2).

4.2.1. Case 1: Heating Dispatch

Under rule-based control (Figure 15), the MGT is dispatched on electrical grounds from 08:00 to 18:00, and its recovered waste heat becomes the primary heat source throughout this window. Heating demand is zero from 00:00 to 05:00, so no heat is supplied during these hours. The demand then rises steeply to its daily maximum at 07:00, a period in

which the MGT has not yet started and the GSHP alone covers the load, tracking demand exactly with no dump. From 08:00 to 18:00 the MGT alone meets the heating load, but the recoverable waste heat exceeds demand in every one of these hours, so a substantial excess is rejected. Once the MGT shuts down, the GSHP alone meets the evening heating load from 19:00 to 22:00, again matching demand exactly with no dump.

In the optimized operation (Figure 16), heat supply follows the price-driven electrical schedule rather than a fixed rule. Heating demand is zero from 00:00 to 05:00, so no heat is supplied during these hours. The demand then rises steeply to its daily maximum at 07:00, a period in which the MGT remains offline and the GSHP alone covers the load, tracking demand exactly with no dump. At 08:00 the MGT comes online and the two units operate together, with recovered waste heat providing the larger share and the GSHP supplying the balance to match the falling demand. From 09:00 to 14:00 the MGT alone meets the heating load, but the recoverable waste heat consistently exceeds it, so a substantial excess is rejected. During the two hours in which the MGT is switched off (15:00–16:00), the GSHP again covers the load directly with no dump. The MGT returns at 17:00, once more with excess heat rejected, and at 18:00 supplies the load almost exactly. From 19:00 to 22:00, with the MGT offline for the remainder of the day, the GSHP meets the entire evening heating demand. Overall, heat dump occurs only in the hours in which the MGT is dispatched on electrical grounds while heating demand is comparatively low, and the GSHP carries a larger share of the daily heating load than under the rule-based strategy.

4.2.2. Case 2: Heating Dispatch

Under rule-based control (Figure 17), the MGT is dispatched on electrical grounds in a single continuous block from 07:00 to 17:00, irrespective of the much lower heating demand in this case. Heating demand is zero from 00:00 to 04:00, so no heat is supplied during these hours. The demand then rises to its daily maximum at 06:00, a period in which the MGT has not yet started and the GSHP alone covers the load, tracking demand exactly with no dump. Once the MGT comes online at 07:00, its recovered waste heat becomes the sole heat source, but the heat available consistently exceeds what the building requires, so the majority is rejected in every hour of the window. After the MGT shuts down, the GSHP alone supplies the modest evening load from 18:00 to 21:00, again matching demand closely with no dump.

Under the optimized dispatch (Figure 18), the MGT is switched on only for the single short, price-driven window identified in the electrical dispatch analysis (07:00–10:00), and the GSHP covers every other hour of the comparatively low heating demand. Heating demand is zero from 00:00 to 04:00, so no heat is supplied during these hours. The demand then rises to its daily maximum at 06:00, which the GSHP alone meets exactly with no dump. At 07:00 the MGT comes online and its recovered waste heat covers the falling demand, with a modest excess rejected. From 08:00 to 10:00, however, demand drops sharply while the MGT continues to run at the level set by the electrical schedule, so the recovered heat far exceeds the building requirement. Once the MGT shuts down at 11:00, the GSHP supplies the entire remaining load through to 21:00, tracking the shallow midday trough and the evening rise closely with no dump. Compared with the rule-based case, the optimized dispatch substantially reduces the dumped heat, since the MGT operating window contracts from eleven hours to four. The GSHP consequently carries the majority of the daily heating load.

4.2.3. Waste Heat Recovery

Table 5 summarizes the daily waste heat balance and the resulting utilization factor for both control strategies in each case. Because the recoverable waste heat is determined

by the electrical dispatch rather than by the building's heat demand, waste heat is dumped whenever the MGT runs at a level whose thermal output exceeds the instantaneous demand. In both cases the day-ahead optimizer shortens the MGT operating window, and the dumped heat falls accordingly. In Case 1 the utilization factor rises from 53% to 69.7%: the usefully recovered heat falls only modestly, from 832.2 to 677.3 kWh/day, while the dumped heat falls far more steeply, from 737.2 to 294.3 kWh/day, because the intervals the optimizer removes are also hours of reduced heating demand. In Case 2 the utilization factor remains low under both strategies, since the heating demand is small relative to the thermal output of the turbine and dumping therefore occurs in every operating hour. It nevertheless doubles, from 15.8% to 31.2%, and the dumped heat falls by roughly three quarters, from 1254.3 to 309.2 kWh/day, as the operating window contracts from eleven hours to four. In both cases, the higher utilization factor therefore reflects a reduction in dumped heat rather than an increase in useful heat recovery, since the usefully recovered heat decreases under the optimized schedule.

Table 5. Waste heat balance and utilization factor for both control strategies.

	Case 1		**Case 2**	
	Rule-Based	**Optimized**	**Rule-Based**	**Optimized**
Total heating demand (kWh/day)	1355.3	1355.3	460.6	460.6
Recoverable exhaust heat (kWh/day)	1569.4	971.6	1489.4	449.6
Usefully recovered heat (kWh/day)	832.2	677.3	235.1	140.4
Dumped heat (kWh/day)	737.2	294.3	1254.3	309.2
Heat supplied by GSHP (kWh/day)	523.1	678.0	225.5	320.2
Waste heat utilization factor (%)	53.0	69.7	15.8	31.2

A consequence of the shorter MGT runtime is that the GSHP assumes a larger share of the heating duty, rising from 523.1 to 678 kWh/day in Case 1 and from 225.5 to 320.2 kWh/day in Case 2. The additional electricity drawn by the heat pump is already reflected in the operating costs reported in Table 4.

5. Conclusions

A day-ahead operation optimization has been developed for a grid-connected microgrid integrating an MGT, a GSHP, and a PV system, supplying the electricity and heating demands of office buildings. Validated dynamic models of the individual components were implemented in Modelica, with the off-design performance of the MGT represented by a data-driven model trained on measured Ansaldo Energia T100 data. A genetic algorithm was used to determine the hourly capacity and on-off status of the turbine over a 24-h horizon, and the resulting schedule was compared with a rule-based control strategy for two representative operating conditions. The two cases represent contrasting operating conditions rather than the full range of conditions over a year, and the results should be interpreted accordingly. In both cases, the day-ahead prices and demand profiles were assumed to be known in advance. The main conclusions are as follows:

- Day-ahead optimization reduced the daily operating cost from 2593.8 to 2257.9 NOK in Case 1 and from 1845.6 to 1222.6 NOK in Case 2, corresponding to reductions of 13% and 33.8% respectively. These savings arise because the optimized schedule is

strongly price-responsive: the turbine is held offline during the low-price overnight hours and intraday price dips and dispatched into the sustained high-price periods, whereas the rule-based strategy follows the building load irrespective of the current electricity price. The larger saving in Case 2 follows from the price profile itself, since prices fall steadily from mid-morning onwards and the rule-based schedule therefore runs the MGT through many hours in which grid import would have cost less than on-site generation.

- Price-driven scheduling also reduced the amount of waste heat dumped by the MGT. The waste heat utilization factor increased from 53% to 69.7% in Case 1 and from 15.8% to 31.2% in Case 2, while the dumped heat fell from 737.2 to 294.3 kWh/day and from 1254.3 to 309.2 kWh/day respectively. The higher utilization factor reflects this reduction in heat dumping rather than an increase in useful heat recovery, since the usefully recovered heat decreased in both cases. This reduction was obtained without any explicit thermal term in the objective function, and arises because the intervals in which the optimizer shuts the turbine down largely align with hours of low heating demand. The shorter turbine runtime does shift a larger share of the heating duty onto the GSHP and thereby increases its electricity consumption, but this effect is fully accounted for in the reported operating costs, so the cost reductions achieved by the optimizer are net of the additional grid electricity drawn by the heat pump.

Future work will extend the analysis to additional days covering all seasons, to further locations and price zones, and to uncertain demand and price forecasts. The schedules obtained with the data-driven MGT model will also be compared with those obtained with constant-efficiency and part-load MGT models, to quantify the value of the off-design representation for scheduling. The sensitivity of the results to the biogas price, the electricity tariff structure and the equipment sizing will also be assessed. In addition, thermal energy storage will be incorporated to decouple electrical dispatch from instantaneous heating demand, and start-up costs and minimum up- and down-time constraints will be included in the optimization so that the trade-off between operating cost and turbine life can be quantified.

Author Contributions: Conceptualization, Q.Z. and M.A.; methodology, Q.Z.; software, R.B. and Q.Z.; validation, Q.Z.; formal analysis, Q.Z.; investigation, Q.Z.; writing—original draft preparation, Q.Z.; writing—review and editing, M.A.; visualization, Q.Z.; supervision, M.A. All authors have read and agreed to the published version of the manuscript.

Funding: This research received no external funding.

Data Availability Statement: The data presented in this study are available on request from the corresponding author.

Conflicts of Interest: The authors declare no conflicts of interest.

Abbreviations

The following abbreviations are used in this manuscript:

AdaGrad	Adaptive Gradient Algorithm
BHE	Borehole Heat Exchanger
BTES	Borehole Thermal Energy Storage
CHP	Combined Heat and Power
DER-CAM	Distributed Energy Resources Customer Adoption Model
ELU	Exponential Linear Unit
ENTSO-E	European Network of Transmission System Operators for Electricity
FFNN	Feedforward Neural Network
GSHP	Ground-Source Heat Pump

HOMER	Hybrid Optimization of Multiple Energy Resources
IWEC	International Weather for Energy Calculations
MAE	Mean Absolute Error
MAPE	Mean Absolute Percentage Error
MGT	Micro Gas Turbine
MSE	Mean Squared Error
NIST	National Institute of Standards and Technology
PV	Photovoltaic
ReLU	Rectified Linear Unit
RMSE	Root Mean Square Error
TRCM	Thermal Resistance and Capacity Model
UPV	Universitat Politècnica de València

The following symbols are used in this manuscript:

Symbols

c_e	Hourly day-ahead electricity price (NOK/kWh)
c_g	Price of biogas (NOK/kWh)
$c_{p,exh}$	Specific heat capacity of the exhaust gas (kJ/(kg·K))
$Cost$	Operation cost of the microgrid (NOK)
$\dot{m}_{exh}$	Exhaust gas mass flow rate (kg/s)
$\dot{m}_{air}$	Combustion air mass flow rate (kg/s)
$\dot{m}_{fuel}$	Fuel mass flow rate (kg/s)
P_{grid}	Power imported from the grid (kW)
P_{GSHP}	Electricity consumption of the GSHP (kW)
P_{load}	Electricity demand of the building (kW)
P_{MGT}	Electrical power output of the MGT (kW)
P_{PV}	PV power generation (kW)
Q_i	Daily energy of heat flow i (kWh)
$\dot{Q}_{avail}$	Rate of recoverable exhaust heat of the MGT (kW)
$\dot{Q}_{dem}$	Heating demand of the building (kW)
$\dot{Q}_{dump}$	Rate of heat rejected to ambient (kW)
$\dot{Q}_{fuel}$	Fuel energy input rate of the MGT (kW)
$\dot{Q}_{GSHP}$	Rate of heat supplied by the GSHP (kW)
$\dot{Q}_{used}$	Rate of usefully recovered heat (kW)
t	Time (h)
T_{exh}	Exhaust gas temperature (°C)
$T_{exh,out}$	Exhaust gas temperature at the heat recovery unit outlet (°C)
$u(t)$	MGT power set-point in hour t (decision variable) (kW)
$\delta(t)$	On/off status of the MGT (–)

Greek symbols

η_{rec}	Waste heat utilization factor (-)

Subscripts

avail	Available (recoverable) exhaust heat
dem	Building heating demand
dump	Heat rejected to ambient
e	Electricity
exh	Exhaust gas
g	Biogas
grid	Electricity grid
h	Hour index
i	Index of heat flow
out	Heat recovery unit outlet
p	Constant pressure
rec	Heat recovery

used Usefully recovered heat

References

1. Berjawi, A.E.H.; Walker, S.L.; Patsios, C.; Hosseini, S.H.R. An evaluation framework for future integrated energy systems: A whole energy systems approach. *Renew. Sustain. Energy Rev.* **2021**, *145*, 111163. [CrossRef]
2. ETN Global. *Micro Gas Turbine Technology Research and Development for European Collaboration*; ETN Global: Brussels, Belgium.
3. Weerakoon, A.H.S.; Assadi, M. Micro Gas Turbines in the Global Energy Landscape: Bridging the Techno-Economic Gap with Comparative and Adaptive Insights from Internal Combustion Engines and Renewable Energy Sources. *Energies* **2024**, *17*, 5457. [CrossRef]
4. Basmadjian, N.; Yun, S.; Hong, Z. Optimization of micro gas turbine based hybrid systems for remote off-grid communities. *Energy Environ.* **2023**, *34*, 1060–1080. [CrossRef]
5. Das, B.K.; Tushar, M.S.H.K.; Zaman, F. Techno-economic feasibility and size optimisation of an off-grid hybrid system for supplying electricity and thermal loads. *Energy* **2021**, *215*, 119141. [CrossRef]
6. Kumar, N.; Karmakar, S. Techno-economics of a trigeneration HRES; a step towards sustainable development. *Renew. Energy* **2022**, *198*, 833–840. [CrossRef]
7. Tsagarakis, K.P.; Efthymiou, L.; Michopoulos, A.; Mavragani, A.; Anđelković, A.S.; Antolini, F.; Bacic, M.; Bajare, D.; Baralis, M.; Bogusz, W.; et al. A review of the legal framework in shallow geothermal energy in selected European countries: Need for guidelines. *Renew. Energy* **2020**, *147*, 2556–2571. [CrossRef]
8. EGEC. *EGEC Geothermal Market Report 2017—Key Findings*; European Geothermal Energy Council: Brussels, Belgium, 2018. Available online: https://www.egec.org/wp-content/uploads/media_publication/MR17_KF_final_web.pdf (accessed on 18 August 2026).
9. Miglani, S.; Orehounig, K.; Carmeliet, J. Integrating a thermal model of ground source heat pumps and solar regeneration within building energy system optimization. *Appl. Energy* **2018**, *218*, 78–94. [CrossRef]
10. Hu, J.; Zheng, W.; Zhang, S.; Li, H.; Liu, Z.; Zhang, G.; Yang, X. Thermal load prediction and operation optimization of office building with a zone-level artificial neural network and rule-based control. *Appl. Energy* **2021**, *300*, 117429. [CrossRef]
11. Figueira, J.S.; García Gil, A.; Vieira, A.; Michopoulos, A.K.; Boon, D.P.; Loveridge, F.; Cecinato, F.; Götzl, G.; Epting, J.; Zosseder, K.; et al. Shallow geothermal energy systems for district heating and cooling networks: Review and technological progression through case studies. *Renew. Energy* **2024**, *236*, 121436. [CrossRef]
12. Zhang, J.; Kong, X.; Shen, J.; Sun, L. Day-ahead optimal scheduling of a standalone solar-wind-gas based integrated energy system with and without considering thermal inertia and user comfort. *J. Energy Storage* **2023**, *57*, 106187. [CrossRef]
13. Chen, W.; Shao, Z.; Wakil, K.; Aljojo, N.; Samad, S.; Rezvani, A. An efficient day-ahead cost-based generation scheduling of a multi-supply microgrid using a modified krill herd algorithm. *J. Clean. Prod.* **2020**, *272*, 122364. [CrossRef]
14. Chen, Z.; Chen, Y.; He, R.; Liu, J.; Gao, M.; Zhang, L. Multi-objective residential load scheduling approach for demand response in smart grid. *Sustain. Cities Soc.* **2022**, *76*, 103530. [CrossRef]
15. Santos, L.H.S.; Silva, J.A.A.; López, J.C.; Arias, N.B.; Rider, M.J.; Da Silva, L.C.P. Integrated Optimal Sizing and Dispatch Strategy for Microgrids Using HOMER Pro. In Proceedings of the 2021 IEEE PES Innovative Smart Grid Technologies Conference—Latin America (ISGT Latin America), Lima, Peru, 15–17 September 2021; pp. 1–5. [CrossRef]
16. Milan, C.; Stadler, M.; Cardoso, G.; Mashayekh, S. Modeling of non-linear CHP efficiency curves in distributed energy systems. *Appl. Energy* **2015**, *148*, 334–347. [CrossRef]
17. Dehghan, B. Performance assessment of ground source heat pump system integrated with micro gas turbine: Waste heat recovery. *Energy Convers. Manag.* **2017**, *152*, 328–341. [CrossRef]
18. Zhang, Q.; Banihabib, R.; Fadnes, F.S.; Sazon, T.A.S.; Ahmed, N.; Assadi, M. Techno-economic analysis of a biogas-fueled micro gas turbine cogeneration system with seasonal thermal energy storage. *Energy Convers. Manag.* **2023**, *292*, 117407. [CrossRef]
19. EnergyPlus. Available online: https://energyplus.net/ (accessed on 17 September 2023).
20. Deru, M.; Field, K.; Studer, D.; Benne, K.; Griffith, B.; Torcellini, P.; Liu, B.; Halverson, M.; Winiarski, D.; Rosenberg, M.; et al. *U.S. Department of Energy Commercial Reference Building Models of the National Building Stock*; National Renewable Energy Laboratory (NREL): Golden, CO, USA, 2011. [CrossRef] [PubMed]
21. Formhals, J.; Hemmatabady, H.; Welsch, B.; Schulte, D.; Sass, I. A Modelica Toolbox for the Simulation of Borehole Thermal Energy Storage Systems. *Energies* **2020**, *13*, 2327. [CrossRef]
22. Ruiz-Calvo, F.; Montagud, C. Reference data sets for validating GSHP system models and analyzing performance parameters based on a five-year operation period. *Geothermics* **2014**, *51*, 417–428. [CrossRef]
23. Tang, C.C. Modeling Packaged Heat Pumps in a Quasi-Steady State Energy Simulation Program. Master's Thesis, Oklahoma State University, Stillwater, OK, USA, 2005.

24. Batzelis, E.I.; Papathanassiou, S.A. A Method for the Analytical Extraction of the Single-Diode PV Model Parameters. *IEEE Trans. Sustain. Energy* **2016**, *7*, 504–512. [CrossRef]
25. Maier, L.; Kratz, M.; Vering, C.; Mehrfeld, P.; Müller, D. Open-source photovoltaic model for early building planning processes: Modeling, application and validation. In Proceedings of the Building Simulation 2021: 17th Conference of IBPSA, Bruges, Belgium, 1–3 September 2021. [CrossRef]
26. Wadood, A.; Ahmed, E.; Rhee, S.B.; Khan, B.S. A Fractional-Order Archimedean Spiral Moth–Flame Optimization Strategy to Solve Optimal Power Flows. *Fractal Fract.* **2024**, *8*, 225. [CrossRef]
27. Wadood, A.; Albalawi, H.; Alatwi, A.M.; Park, H. Modified Swarm-Based Artificial Intelligence Optimization for Optimal Coordination of Directional Overcurrent Relays in Power System. *IEEE Access* **2025**, *13*, 71007–71026. [CrossRef]
28. ENTSO-E. ENTSO-E Transparency Platform. Available online: https://transparency.entsoe.eu/ (accessed on 18 August 2026).
29. Lyse Energi AS. Personal communication at the Future Energy Hub Seminar, Stavanger, Norway, 2024.

Disclaimer/Publisher's Note: The statements, opinions and data contained in all publications are solely those of the individual author(s) and contributor(s) and not of MDPI and/or the editor(s). MDPI and/or the editor(s) disclaim responsibility for any injury to people or property resulting from any ideas, methods, instructions or products referred to in the content.